IEEE Photonics Journal
An IEEE Photonics Society Publication

Open Access

# Fully Planarized Perfect Metamaterial Absorbers With No Photonic Nanostructures

Volume 8, Number 1, February 2016

Yan Kai Zhong
Sze Ming Fu
Nyan Ping Ju
Ming-Hsiang Tu
Bo-Ruei Chen
Albert Lin

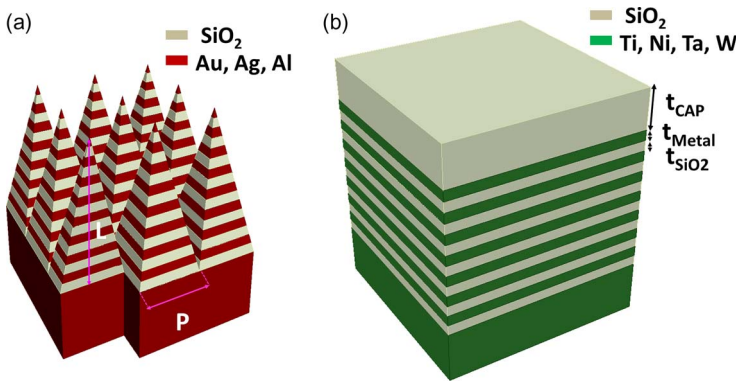


DOI: 10.1109/JPHOT.2015.2507368
1943-0655 

IEEE photonics SOCIETY

IEEE

# Fully Planarized Perfect Metamaterial Absorbers With No Photonic Nanostructures

**Yan Kai Zhong, Sze Ming Fu, Nyan Ping Ju, Ming-Hsiang Tu, Bo-Ruei Chen, and Albert Lin**

Department of Electronic Engineering, National Chiao Tung University, Hsinchu 30010, Taiwan

*DOI: 10.1109/JPHOT.2015.2507368*


Manuscript received November 17, 2015; revised December 4, 2015; accepted December 7, 2015. Date of publication December 9, 2015; date of current version December 22, 2015. Corresponding author: A. Lin (e-mail: hdtd5746@gmail.com).

**Abstract:** In the past, perfect metamaterial absorbers (PMAs) have required nanolithography patterning to boost broadband absoprtion. Tapered structures, in particular, are shown to achieve close-to-unity absorption over broadband using adiabatic light coupling. A nontapered PMA is desirable due to the fact that it is easier to fabricate using regular lithography techniques. This facilitates the scalability to large-area photonic applications such as thermophotovoltaics. In this work, we propose a fully planarized design with ultrathin metallic films for broadband PMAs. The design provides close-to-unity absorbance over a wide spectral range and is wavelength scalable from middle ultraviolet to long wavelength infrared. The planarized design is extremely easy to fabricate, and it requires no lithography nor etching. The design can be used with different moderate-extinction metals such as tungsten, titanium, tantalum, and nickel. The physics is that the thin layer of the moderate-extinction metal allows photons to penetrate through itself. The insertion of the dielectric between thin metal layers is necessary to spatially separate the ultrathin metallic thin film to boost the effect of thin-film absorption. As far as the bandwidth normalized to center wavelength is concerned, we believe that the experimental result demonstrated here shows the broadest bandwidth to date.

**Index Terms:** Metamaterials, photovoltaic, silicon nanophotonics, optical properties of photonic materials.

## 1. Introduction

Perfect metamaterial absorbers (PMA) [1]–[10] have been an important research subject due to the potential applications in diverse applications in nano-photonics [11]–[17]. These include biomedical optics [1], [18]; ultra-high sensitivity sensing [13]; antenna systems [15]; cloaking [12]; radar cross section (RCS) reduction [19]; thermal emitters [16]; and thermophotovoltaics (TPV) [17]. Previously, the perfect absorption is realized by using silver (Ag), gold (Au), and aluminum (Al) through different design methodologies. The physics behind these perfect absorbers in literature includes plasmonics, adiabatic coupling, and mode excitations. The significant effort using silver plasmonics-based design is proposed by Atwater *et al.* [5]. The ultra-thin metal-dielectric-metal configuration provides broadband absorption in the visible wavelength regime using silver plasmonic mode excitations. Afterward, a close-to-unity absorption over broadband was proposed by Fang *et al.* [9], [10] using adiabatically coupled nano-tip arrays with the aid of hyperbolic

meta-materials (HMMs). This is the most pronounced effort for the broadband metamaterial absorbers to date since the absorption bandwidth is unprecedentedly wide. The hyperbolic meta-material is an artificial material with a metal-like permittivity in one direction and a dielectric-like permittivity in another direction [20]–[32]. The physics behind the tapered hyperbolic meta-material absorbers is that the incoming light is coupled into the tapered HMM waveguiding structure. In order to achieve a broad absorption band, a layer-by-layer metal-dielectric nanotip structure is used, and the photons with longer wavelengths are absorbed in the lower part of the tapered HMM stack while the photons with shorter wavelengths are absorbed in the upper part of the tapered HMM stack. The reason that a tapered structure is necessary to realize the broadband absorption is the reduction of the reflections due to the gradually varied effective index associated with the nanotips. Only in this way, photons with different wavelengths can all be gradually coupled into the HMM stack.

The fact that the HMM nanotip design employs a tapered sidewall to boost the absorption may prevent the feasibility for large-area applications including thermophotovoltaics (TPV). The fabrication of a precisely tapered structure can be time-consuming, and repeated lithography and etching steps have to be conducted to realize such a structure using focused ion beam (FIB) [10]. In this work, we proposed a planarized design for metamaterial absorbers. Different from previous broadband perfect metamaterial absorber designs where high extinction metals such as Au, Ag, and Al are used for enhanced absorption, moderate-extinction metals are used to realize perfect absorption. The physics utilized here is the field penetration and field dissipation at the ultra-thin metallic films. In order to have this penetration effect, using moderate-extinction metals is necessary. Since previously in literature the broadband perfect absorbers are all realized using plasmonics, guided resonances, or adiabatic coupling in hyperbolic meta-materials, the proposal in this work provides a novel design and new physics for the implementation of a broadband absorber. Compared to tapered HMM perfect absorbers, this design eliminates the need for lithography and etching and, therefore, totally scalable to large-area photonic applications. Similar to nano-tip HMM PMAs proposed by Fang *et al.* [9], [10], our design also possesses broad absorption bandwidth with wavelength scalability, and its broadband absorption can be tuned to cover different wavelength regimes ranging from middle ultraviolet (MUV) to long wavelength infrared (LWIR).

## 2. The All-Planar Structure Based on Moderate-Extinction Metals

For the realization of the proposed planar PMAs, the selection of lower extinction metals such as titanium (Ti), tungsten (W), and nickel (Ni) is essentially critical to have field penetration through the ultra-thin metallic layers. The gold (Au), silver (Ag), or even aluminum (Al) in general has higher extinction in its dielectric function, and its high extinction coefficient leads to excessive reflection. For the case of Au-, Ag-, or Al- based PMAs, the physics is the mode coupling that in turn initiates the strong absorption in the metallic materials. This is evident from the field profiles in previous literature [9], [10] that the incoming field is penetrating into the metal film from the side. In the case of our design using planarized metal-dielectric stacks, the field has to penetrate the metal thin-film from the top. This means the metal extinction coefficient ($k$) cannot be too large. Otherwise, significant reflection will exist even at a very thin metallic layer thickness. This point will be evident below when we compare the spectral absorption for different metals with various $k$ values.

As illustrated in Fig. 1, the structure consists of repeated dielectric-metal stacks. The refractive index ($n$) and extinction coefficients ($k$) from Rsoft material database are used in this study [33]. The Lorentz-Drude dielectric functions are used to describe the metal $n$–$k$ in the database. The rigorously coupled wave analysis (RCWA) using Diffractmod is used to calculate the spectral absorbance. The Diffractmod is different from the traditional Fourier Modal Method (FMM) in the aspect that the expansion basis is the eigen modes in the layered periodic waveguide structures. Using eigen modes of the structure itself to expand the solution fields is more natural.

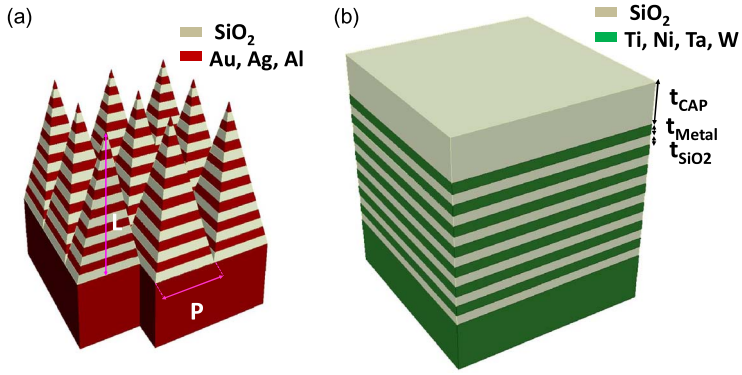


Fig. 1. (a) Nanotip hyperbolic metamaterial (HMM) perfect metamaterial absorber (PMA) based on high-extinction metals such as gold (Au), silver (Ag), and aluminum (Al) [9]. (b) Proposed fully planarized ultra-thin-metal PMAs based on moderate-extinction metals, such as titanium (Ti), nickel (Ni), tungsten (W), and ruthenium (Ru).

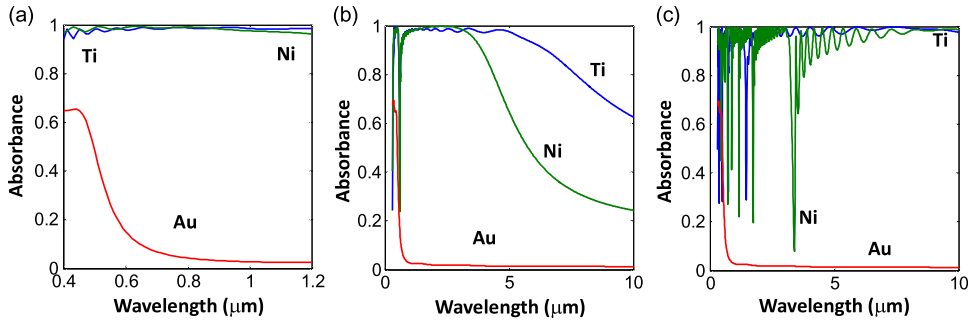


Fig. 2. Spectral responses of fully planarized PMAs using Ti, Ni, or Au over different wavelength ranges. The high extinction of Au prevents the field penetration through the ultra-thin metallic films. The wavelength scalability is from MUV to LWIR. For geometrical dimensions, (a) $t_{Metal} = 2.6$ nm, $t_{SiO2} = 91.8$ nm, and $t_{CAP} = 91.8$ for Ti PMA. $t_{Metal} = 2$ nm, $t_{SiO2} = 50$ nm, and $t_{CAP} = 50$ nm for Ni PMA. $t_{Metal} = 2$ nm, $t_{SiO2} = 50$ nm, and $t_{CAP} = 50$ nm for Au PMA. (b) $t_{Metal} = 2.6$ nm, $t_{SiO2} = 200$ nm, and $t_{CAP} = 200$ nm for Ti PMA. $t_{Metal} = 2$ nm, $t_{SiO2} = 200$ nm, and $t_{CAP} = 200$ nm for Ni PMA. $t_{Metal} = 2$ nm, $t_{SiO2} = 200$ nm, and $t_{CAP} = 200$ nm for Au PMA. (c) $t_{Metal} = 2$ nm, $t_{SiO2} = 500$ nm, and $t_{CAP} = 500$ nm for Ti PMA. $t_{Metal} = 1$ nm, $t_{SiO2} = 1200$ nm, and $t_{CAP} = 1200$ nm for Ni PMA. $t_{Metal} = 2$ nm, $t_{SiO2} = 1000$ nm, and $t_{CAP} = 1000$ nm for Au PMA. There are 16 pairs (16X) of metal-dielectric in this calculation.

This leads to significantly improved convergence, especially in the presence of metallic layers in the calculation domains.

## 3. The Proposal of Moderate-Extinction PMAs Using Successive Field Penetrations

The spectral responses for fully-planarized PMAs implemented with different metals, including Ti, Ni, and Au, are shown in Fig. 2. The wavelength scalability is also demonstrated from Fig. 2(a)–(c). The higher extinction of Au prevents the possibility of fully planarized PMAs using Gold. The physical reason is that the higher-extinction metals lead to strong reflection even at an ultra-thin thickness. Further reducing the thickness of high-extinction metals may alleviate this issue, but this may lead to the need for atomic layer deposition (ALD) or molecular beam epitaxy (MBE) for the thickness below 2 nm. Using e-gun evaporation or sputtering seems to be impractical for the thickness below several nanometers. In the case of Ni, the absorption is slightly lower than Ti. The physical reason is that the extinction of nickel is slightly higher than titanium. This leads to reduced bandwidth, evident from Fig. 2(b), where the field penetration becomes ineffective for the Ni PMA

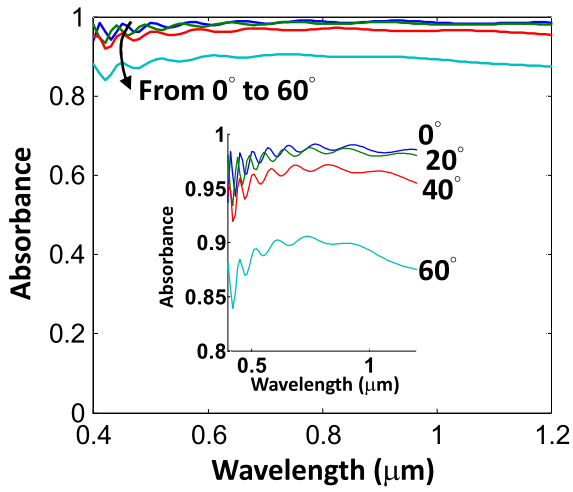


Fig. 3. Spectral absorbance versus wavelength for various incidence angles in the case of the titanium (Ti) PMA. The geometry is the same as the Ti PMA in Fig. 2(a), i.e., $t_{Metal} = 2.6$ nm, $t_{SiO2} = 91.8$ nm, and $t_{CAP} = 91.8$. There are 16 pairs (16X) of metal-dielectric in this calculation.

at $\lambda > 3$ $\mu$m, while the Ti PMA can sustain until $\lambda = 5$ $\mu$m. This point will become clearer below when the spectral absorption versus material *n–k* is calculated for fully-planarized PMAs. It should be emphasized that although lower extinction is generally preferable for our design due to lower reflection from the metal films and easier penetration through the metal thin-films, there is slight variation in the broadband absorption in the regime of low-extinction *k* values. As a result, there are optimal values for material *n–k*, evident from the discussion below. The scaling toward long wavelength is primarily by adjusting the dielectric layer thickness. The metallic layer thickness can be kept unchanged since the ultra-thin metal layer thickness is the key to the successive field penetrating and the absorption in the periodic dielectric-metallic layered structure. Fig. 3 shows the spectral absorbance, at oblique incidence angles, versus wavelength for the Ti PMA in Fig. 2(a). It can be seen that the broadband high absorption still exists for large incident angles. The absorbance degrades to around 0.9 for the case of 60° incidence. The physical reason that there is only slight degradation at oblique incidence is due to the fact that the broadband high absorption is based on the field penetration and absorption at the ultra-thin metal films. This phenomenon will not change significantly with the incident angles, and this results in reasonably high absorption for varying incidence angles. The slight degradation of the absorption value at large incident angles is due to the effective path length for photons becomes longer in the metal-dielectric multilayer structure. Therefore, the effective metal thickness perceived by the photons becomes greater. In this scenario, the ultra-thin metal field penetration can slightly be affected due to the effectively greater metal film thickness.

The fact that moderate or low-extinction metals are needed is very important for the design of fully-planarized PMAs. We investigate the effect of material *n–k* on the characteristics of fully-planarized PMAs in Fig. 4. It is clear from Fig. 4(a) that when material *k* value becomes too high, the absorbance begins to decrease. In this scenario, the incident field cannot penetrate through the metal thin-film thoroughly, and the reflection is significant. For material *k* value that is too low, the absorption is insufficient, and this leads to lower absorbance value. Increasing the metal layer thickness can be a cure for excessively low *k* value. This is demonstrated in Fig. 4(b), where the $t_{Metal}$ is increased from 2 nm to 5 nm. It can be seen that the optimal *k* shifted from $k = 4$ toward a lower value around $k = 2$. Greater $t_{Metal}$ value can be beneficial for thin-film deposition since for 5 nm metal thickness, it is easier to control thin-film uniformity using e-gun evaporator compared to the 2 nm metal thickness. Nonetheless, the material *n–k* is naturally decided. As a result, the choice of *n–k* cannot be totally arbitrary. Based on our survey of different metals, including Ag, Au, Al, Ni, Ti, and W, titanium (Ti) provides the best PMA

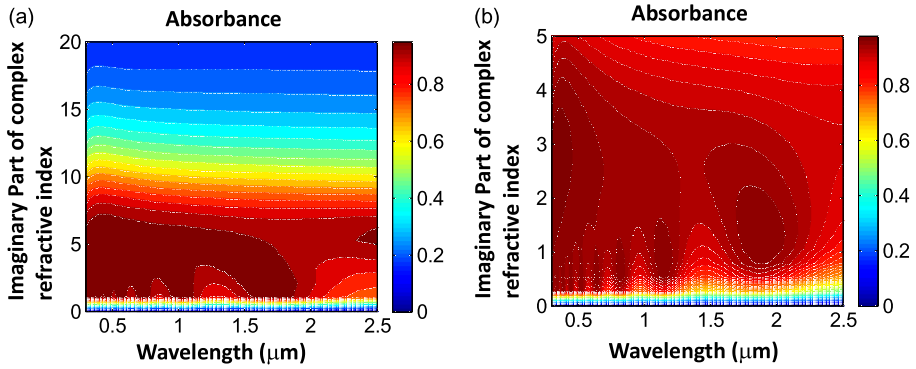


Fig. 4. Fully planarized PMA absorbance versus the metallic material extinction coefficient ($k$). The metallic refractive index ($n$) is set as 3. The geometry dimension is (a) $t_{Metal} = 2$ nm, $t_{SiO2} = 50$ nm, and $t_{CAP} = 50$ nm. (b) $t_{Metal} = 5$ nm, $t_{SiO2} = 50$ nm, and $t_{CAP} = 50$ nm. There are 16 pairs (16X) of metal-dielectric in this calculation.

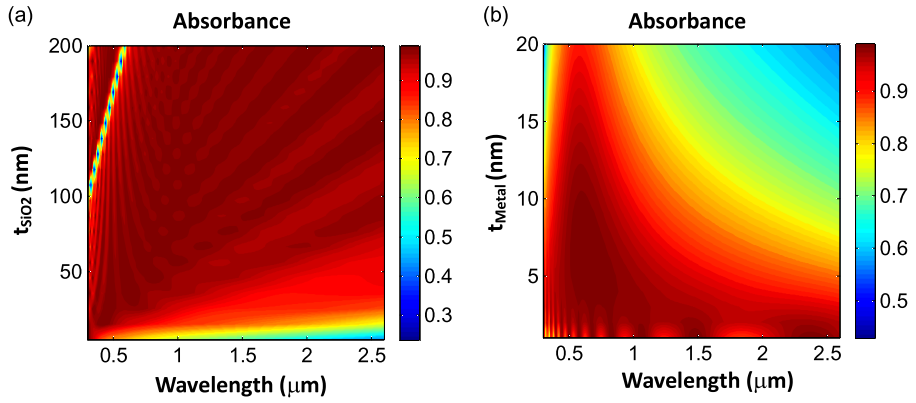


Fig. 5. (a) Fully planarized Ti PMA absorbance versus the $SiO_2$ layer thickness ($t_{SiO2}$). $t_{Metal} = 2$ nm. $t_{CAP} = t_{SiO2}$. (b) Fully planarized Ti PMA absorbance versus the Ti layer thickness ($t_{Metal}$). $t_{SiO2} = 80$ nm. $t_{CAP} = 80$ nm. There are 16 pairs (16X) of metal-dielectric in this calculation.

characteristics, but the optimal thickness is around 2 nm. Other new materials can be synthesized and evaluated with better $k$ value dispersion, matching to the need of a specific broadband absorption application. This can potentially provide thicker optimal $t_{Metal}$ that eliminates the difficulty when depositing ultra-thin metallic layers.

Fig. 5(a) shows the spectral absorbance contour plot versus $SiO_2$ dielectric layer thickness ($t_{SiO2}$) for Ti planar PMAs. It can be seen from Fig. 5(a) that when $t_{SiO2}$ is gradually increased, the wide absorption band is gradually shifted toward longer wavelengths. Additionally, at $t_{SiO2} < 10$ nm, the wide absorption band can disappear. This is due to the fact that in this case, the metallic thin-layers are too closely spaced and in the extreme case at $t_{SiO2} = 0$ nm, the bulk property of the metal will be seen. In this case, an ultra-thin metallic PMA no longer exists. Another explanation for the absence of the wide absorption band at $t_{SiO2} < 10$ nm is along the line of the cancelation of the reflected wave. The reflected wave from each interface, in fact, cancels each other due to the phase differences. This phenomenon results in a very low reflectance and a very high absorbance for the fully planarized PMAs proposed here. For the case of $t_{SiO2} < 10$ nm, the destructive interference condition for the reflected waves can no longer be supported in the target wavelength range for a specific PMA design. The quarter-wavelength $t_{SiO2}$ can be beneficial for the cancelation of the reflected waves by the adjacent metallic thin-layers. In this regard, $t_{SiO2} < 10$ nm is too thin for the wavelength range from 0.3 $\mu$m to 2.6 $\mu$m. Fig. 5(b) shows the spectral absorbance

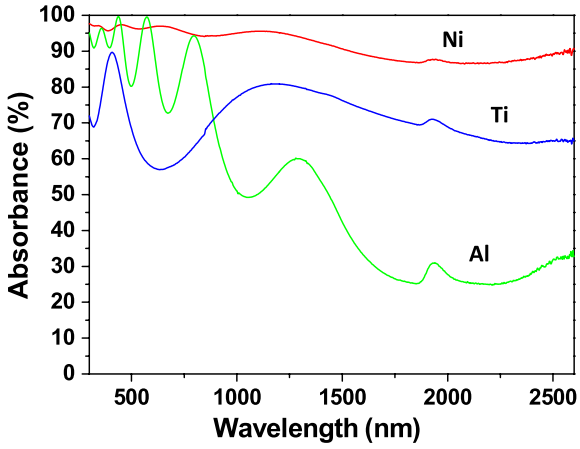


Fig. 6. Spectral absorption of various metals implemented into 16-pair (16x) fully planarized PMAs. The $SiO_2$ thickness ($t_{SiO2}$) is uniformly 30 nm, and the metal thickness ($t_{Metal} = 2$ nm) is 2 nm. $t_{CAP} = 40$ nm.

contour plots versus metallic layer thickness ($t_{Metal}$) for Ti planar PMAs. It can be seen that at a thicker metal layer thickness, the wide absorption band again gradually disappears. This is due to the fact that at greater $t_{Metal}$, the field penetration is no longer pronounced. Similarly, in the extreme case of very large $t_{Metal}$, the bulk property of the metallic material is seen. This happens when $t_{Metal}$ is greater than the skin depth of the metallic material used in the perfect metamaterial absorber.

## 4. Experimental Result Using Ti/$SiO_2$ Perfect Metamaterial Absorbers

The preliminary experiment effort has been established to investigate the broadband characteristics for the fully planarized PMAs. The alternating metal/$SiO_2$ stacking is deposited for different metallic materials including Ni, Ti, and Al, as shown in Fig. 6. A silicon wafer is used as the substrate. For the samples in Figs. 6 and 7, a 200 nm metallic layer is deposited on top of the silicon substrate to prevent any transmission into the substrate and to serve as a bottom plate. For the case of Fig. 6, zero transmission is measured. Nevertheless, for the case of Fig. 7, we see slight transmission around 8% from $\lambda = 1500$ nm to $\lambda = 2600$ nm. As a result, a metallic layer is deposited on the backside of the Si wafer to eliminate the wave escape. In fact, this is unnecessary if the 200 nm metal layer on top of the Si wafer is further increased in thickness. The fabrication does not count on lithography or reactive ion etching (RIE) of any kinds. The multitarget electron-gun (e-gun) evaporation is used to deposit Ni, Ti, Al, and SiO. The deposition pressure is around $3 \times 10^{-6}$ torr, and no heating to the substrate is applied during the deposition. The deposited metal thickness is 2 nm, which is a very thin thickness for e-run evaporators, and, therefore, the uniformity is certainly not very satisfactory. The measurement of the absorbance is achieved by using a Hitachi U-4100 ultraviolet-visible-near-infrared (UV-VIS-NIR) spectrometer with an integration sphere. The light source is a quickly mountable type deuterium lamp for the ultraviolet region and a 50 W halogen lamp for the visible-near-infrared region. The pre-monochromator is Littrow monochromator using a diffraction grating, and the main monochromator is also of the grating type with two switchable diffraction gratings. The detector is photomultiplier for the UV-VIS region and a cooling type PbS photoconductive detector for the NIR region.

The thickness of the $SiO_2$ layer in Fig. 6 is chosen to be 30 nm for Ni, Ti, and Al samples. It can be seen from Fig. 6 that Ti and Ni samples provide decent broadband absorption characteristics. As far as the absorption bandwidth normalized to the center wavelength is concerned, we believe the measured result here is the broadest bandwidth PMAs experimentally demonstrated to date [5], [9], [10]. For the Al sample, the extinction coefficient of Al is excessively high for implementing perfect absorption using a planarized structure. Strong reflection exists for Al thin-film, especially

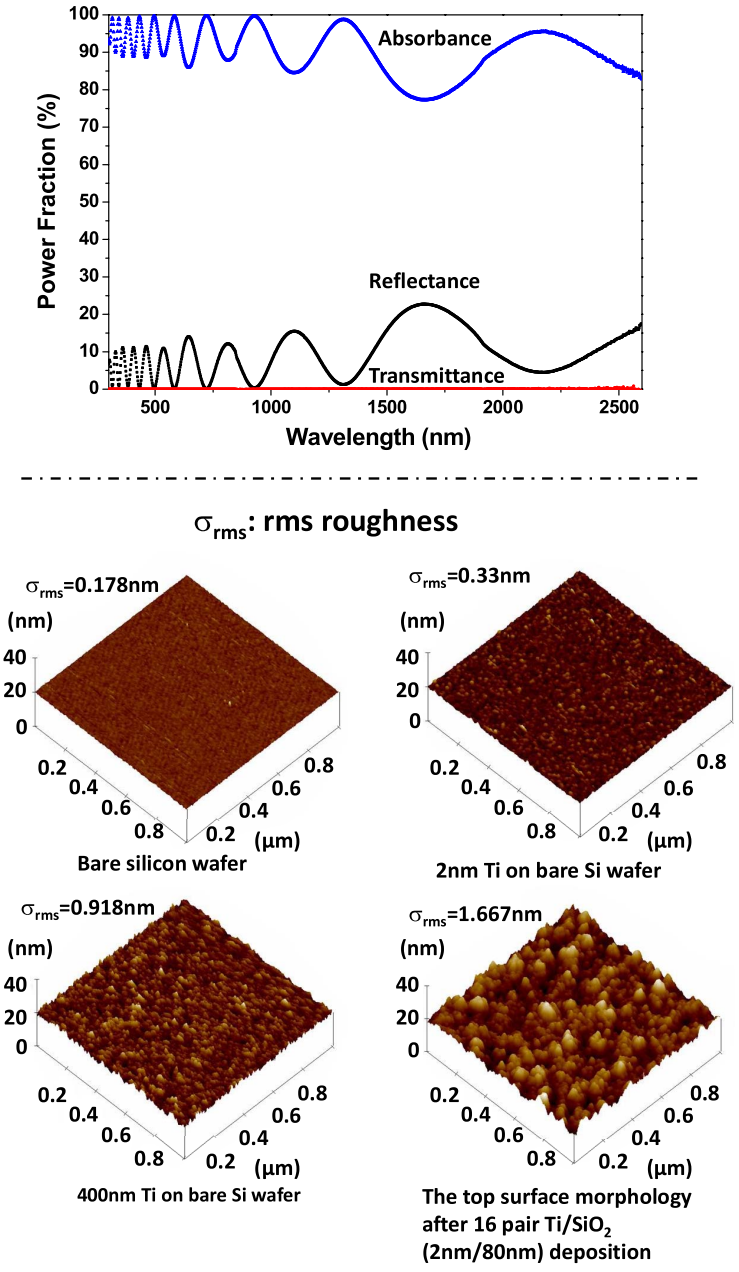


Fig. 7. Spectral response of 16-pair (16X) Ti fully planarized PMAs for $SiO_2$ thickness of $t_{SiO2} =$ 80 nm and Ti thickness of $t_{Metal} = 2$ nm. $t_{CAP} = 80$ nm. The AFM images and root-mean-square (RMS) roughness at different stages of deposition are also provided.

beyond $\lambda = 1$ $\mu$m. In Fig. 7, the $SiO_2$ thickness is increased to $t_{SiO2} = 80$ nm to further boost the absorption, suggested by the simulation result in Fig. 2(a). $t_{SiO2} = 80$ nm is more suitable for the wave interference and the field penetration if the target wavelength is chosen as from visible to near infrared, i.e. $\lambda = 0.4$ $\mu$m $- 1.2$ $\mu$m. The slight degradation of the measured absorbance from the perfect close-to-unity value is due to the finite surface roughness for e-gun deposited films. In addition to the absorbance data, the surface morphology data is also provided with atomic force microscope (AFM) images and the corresponding root-mean-square (RMS) roughness values in Fig. 7. The AFM images show the surface morphology for the Ti films of different thickness and for the top surface of the finished 16-pair stack. The surface roughness increases

with the number of the deposited pairs, and this results in a slight deviation of the experimental results from the calculated ones. The surface roughness leads to random light scattering that can degrade the designed field penetration and absorption. In this case, there can be non-negligible non-specular diffraction power, which increases the reflection at certain wavelengths. As a result, the pure phenomenon of 1-D field penetration through the ultra-thin metallic films is affected, and this leads to a lowered absorbance value. Nonetheless, the measured high absorption indicates the proposed fully planarized design can in fact tolerate large process deviations and surface roughness. To have more uniform ultra-thin metallic thin layers and unity absorption over broadband, atomic layer deposition (ALD), metalorganic chemical vapor deposition (MOCVD), or molecular beam epitaxy (MBE) can be used for Ti thin-layer deposition. Unfortunately, although the available ALD in our nano-fabrication facility allows for Ti, titanium nitride (TiN), hafnium oxide ($HfO_2$), and aluminum oxide ($Al_2O_3$) deposition, it is not allowed to load samples with Ti thin films into the $HfO_2$ chamber. As a result, we use evaporated Ti and $SiO_2$ as an example, to demonstrate the effectiveness of our design. It should be emphasized that the robustness to the process and geometry variation is very important for nano-photonic applications. From this point of view, one-dimensional planar structures proposed in this work are preferable, compared to the two-dimensional nano-structured metamaterial stacks since the quasi-guided mode excitations in two-dimensional photonic nanostructures can depend more on the dimension and geometry.

## 5. Conclusion

In this work, we propose a fully planarized perfect metamaterial absorber, which is beneficial for a wide range of photonic applications due to the elimination of the need for lithography and etching, the scalability for large-area device fabrications, the wavelength scalability, and the simple numerical analysis. The key requirement for the realization of such a structure is identified as the moderate-extinction coefficient for the metallic materials. The high-extinction metal such as gold (Au), silver (Ag), or aluminum (Al), leads to excessive reflection even at an ultra-thin thickness. On the other hand, many refractory metals suitable for thermophotovoltaics (TPV), such as tungsten (W), titanium (Ti), and tantalum (Ta), exhibit moderate extinction coefficients, and can be used for the realization of fully planarized PMAs. The analysis using rigorously coupled wave analysis (RCWA) clearly demonstrates the wavelength scalability of our designs. The material $n$–$k$ criterion is investigated, and it is concluded that the $k$ values in the range of 3 are the most suitable for the planar PMAs realized with 2 nm metal thin-film. The underlying physics can be explained using the successive field penetration and field absorption, provided that the metallic layer thickness is smaller than its skin depth. The experimental result using $Ti/SiO_2$ stacking clearly demonstrates the physical principles, and in fact the proposed design works very well in practice. The future effort will be devoted to the improvement of the thin-film morphology and uniformity. We believe the experimental result here provides a broadest bandwidth PMA to date.

## References

[1] C. M. Watts, X. Liu, and W. J. Padilla, "Metamaterial electromagnetic wave absorbers," *Adv. Opt. Mater.*, vol. 24, no. 23, pp. OP98–OP120, Jun. 2012.
[2] H. Tao *et al.*, "A metamaterial absorber for the terahertz regime: Design, fabrication and characterization," *Opt. Exp.*, vol. 16, no. 10, pp. 7181–7188, May 2008.
[3] X. Liu, T. Starr, A. F. Starr, and W. J. Padilla, "Infrared spatial and frequency selective metamaterial with near-unity absorbance," *Phys. Rev. Lett.*, vol. 104, no. 20, May 2010, Art. ID 207403.
[4] Y. Avitzour, Y. A. Urzhumov, and G. Shvets, "Wide-angle infrared absorber based on a negative-index plasmonic metamaterial," *Phys. Rev. B, Condens. Matter Mater. Phys.*, vol. 79, no. 4, Jan. 2008, Art. ID 045131.
[5] K. Aydin, V. E. Ferry, R. M. Briggs, and H. A. Atwater, "Broadband polarization-independent resonant light absorption using ultrathin plasmonic super absorbers," *Nat. Commun.*, vol. 2, no. 10, Dec. 2011, Art. ID 517.
[6] H. Tao *et al.*, "Highly flexible wide angle of incidence terahertz metamaterial absorber: Design, fabrication, and characterization," *Phys. Rev. B, Condens. Matter Mater. Phys.*, vol. 78, no. 24, Dec. 2008, Art. ID 241103.
[7] H. Tao *et al.*, "A dual band terahertz metamaterial absorber," *J. Phys. D, Appl. Phys.*, vol. 43, no. 22, May 2010, Art. ID 225102.

[8] J. Hao *et al.*, "High performance optical absorber based on a plasmonic metamaterial," *Appl. Phys. Lett.*, vol. 96, no. 25, Jun. 2010, Art. ID 251104.
[9] Y. Cui *et al.*, "Ultrabroadband light absorption by a sawtooth anisotropic metamaterial slab," *Nano Lett.*, vol. 12, no. 3, pp. 1443–1447, Mar. 2012.
[10] D. Ji *et al.*, "Broadband absorption engineering of hyperbolic metafilm patterns," *Sci. Rep.*, vol. 4, 2014, Art. ID 4498.
[11] X. Zhang and Z. Liu, "Superlenses to overcome the diffraction limit," *Nat. Mater.*, vol. 7, no. 6, pp. 435–441, Jun. 2008.
[12] D. Schurig *et al.*, "Metamaterial electromagnetic cloak at microwave frequencies," *Science*, vol. 314, no. 5801, pp. 977–980, Nov. 2008.
[13] N. Liu, M. Mesch, T. Weiss, M. Hentschel, and H. Giessen, "Infrared perfect absorber and its application as plasmonic sensor," *Nano Lett.*, vol. 10, no. 7, pp. 2342–2348, Jul. 2010.
[14] H.-T. Chen *et al.*, "A metamaterial solid-state terahertz phase modulator," *Nat. Photon.*, vol. 3, no. 3, pp. 148–151, Mar. 2009.
[15] D. Dregely *et al.*, "3D optical Yagi–Uda nanoantenna array," *Nat. Commun.*, vol. 2, no. 4, Apr. 2010, Art. ID 267.
[16] X. Liu *et al.*, "Taming the blackbody with infrared metamaterials as selective thermal emitters," *Phys. Rev. Lett.*, vol. 107, no. 4, Jul. 2011, Art. ID 045901.
[17] C. Wu *et al.*, "Metamaterial-based integrated plasmonic absorber/emitter for solar thermo-photovoltaic systems," *J. Opt.*, vol. 14, no. 2, Jan. 2012, Art. ID 024005.
[18] W. H. Emerson, "Electromagnetic wave absorbers and anechoic chambers through the years," *IEEE Trans. Antennas. Propag.*, vol. AP-21, no. 4, pp. 484–490, Jul. 1973.
[19] B. A. Munk, *Frequency Selective Surfaces: Theory and Design*. New York, NY, USA: Wiley, 2000.
[20] V. G. Veselago, "The electrodynamics of substances with simultaneously negative values of $\varepsilon$ and $\mu$," *Sov. Phys. Uspekhi.*, vol. 10, no. 4, pp. 509–514, 1968.
[21] D. R. Smith and D. Schurig, "Electromagnetic wave propagation in media with indefinite permittivity and permeability tensors," *Phys. Rev. Lett.*, vol. 90, no. 7, Feb. 2003, Art. ID 077405.
[22] I. V. Lindell, S. A. Tretyakov, K. I. Nikoskinen, and S. Ilvonen, "BW media—Media with negative parameters, capable of supporting backward waves," *Microw. Opt. Technol. Lett.*, vol. 31, no. 2, pp. 129–133, Oct. 2001.
[23] P. A. Belov, "Backward waves and negative refraction in uniaxial dielectrics with negative dielectric permittivity along the anisotropy axis," *Microw. Opt. Technol. Lett.*, vol. 37, no. 4, pp. 259–263, May 2003.
[24] R. K. Fisher and R. W. Gould, "Resonance cones in the field pattern of a short antenna in an anisotropic plasma," *Phys. Rev. Lett.*, vol. 22, no. 21, pp. 1093–1095, May 1969.
[25] L. V. Alekseyev, V. A. Podolskiy, and E. E. Narimanov, "Homogeneous hyperbolic systems for terahertz and far-infrared frequencies," *Adv. Optoelectron.*, vol. 2012, 2012, Art. ID 267564.
[26] M. Noginov, M. Lapine, V. Podolskiy, and Y. Kivshar, "Focus issue: Hyperbolic metamaterials," *Opt. Exp.*, vol. 21, no. 12, pp. 14895–14897, Jun. 2013.
[27] Z. Jacob, I. I. Smolyaninov, and E. E. Narimanov, "Broadband Purcell effect: Radiative decay engineering with metamaterials," *Appl. Phys. Lett.*, vol. 100, no. 18, Apr. 2012, Art. ID 181–105.
[28] S.-A. Biehs, M. Tschikin, and P. Ben-Abdallah, "Hyperbolic metamaterials as an analog of a blackbody in the near field," *Phys. Rev. Lett.*, vol. 109, no. 10, Sep. 2012, Art. ID 104301.
[29] J. Li, L. Fok, X. Yin, G. Bartal, and X. Zhang, "Experimental demonstration of an acoustic magnifying hyperlens," *Nat. Mater.*, vol. 8, no. 12, pp. 931–934, Dec. 2009.
[30] I. I. Smolyaninov and E. E. Narimanov, "Metric signature transitions in optical metamaterials," *Phys. Rev. Lett.*, vol. 105, no. 6, Aug. 2010, Art. ID 067402.
[31] I. I. Smolyaninov, Y.-J. Hung, and E. Hwang, "Experimental modeling of cosmological inflation with metamaterials," *Phys. Lett. A*, vol. 376, no. 38/39, pp. 2575–2579, Aug. 2012.
[32] I. I. Smolyaninov and A. V. Kildishev, "Light propagation through random hyperbolic media: From a pile of sand to large scale structure of present day universe," *Opt. Lett.*, vol. 38, no. 6, pp. 971–973, Mar. 2013.
[33] *Rsoft, Rsoft CAD User Manual*, 8.2 ed. New York, NY, USA: Rsoft, 2010.